Synthesis of Fe_3O_4@m-SiO_2 nanocomposites using Rice Husk Ash derived SiO_2

Nazli Aharipour [a], Adrine Malek Khachatourian [a*], Ali Nemati [a]

[a] Department of Materials Science and Engineering, Sharif University of Technology, Tehran, Iran.

[*]**Corresponding author email:** <u>khachatourian@sharif.edu</u>

Abstract

Fe_3O_4 nanoparticles (NPs) with a continuous and mesoporous silica (m-SiO_2) shell were synthesized using a one-step method, sourcing silica from rice husk ash (RHA). The rice husk was thermally treated to obtain ash, from which silica was extracted as sodium silicate and precipitated by pH reduction. This silica powder, combined with iron chloride salts, facilitated the synthesis of the core-shell NPs. Mint extract acted as a capping agent to prevent agglomeration, and CTAB (cetyltrimethylammonium bromide) was used to create the porous SiO_2 shell. X-ray diffraction (XRD), Field emission scanning electron microscopy (FESEM), and transmission electron microscopy (TEM) characterization investigated the structure, size, and shell formation. Coating integrity and suspension stability were assessed through Fourier transform infrared spectroscopy (FTIR) and dynamic light scattering (DLS). DLS analysis showed a relatively narrow particle size distribution with an average hydrodynamic size of 72.6 nm. Small-angle X-ray scattering (SAXS) provided insights into the meso- and nanoscale structure, while BET and nitrogen adsorption-desorption isotherms confirmed the mesoporous nature of the silica shell. Magnetization measurements showed superparamagnetic behavior, with specific magnetization values of 57.9 emu/g for Fe_3O_4 and 27.5 emu/g for Fe_3O_4@m-SiO_2. These results confirm the successful synthesis of superparamagnetic magnetite NPs with a mesoporous silica coating from RHA.

Keywords: Core-shell nanoparticles; Fe_3O_4; porous SiO_2 shell; rice husk ash; superparamagnetic; magnetization.

1

1- Introduction

Nanotechnology involves studying, controlling, and manipulating materials at the nanoscale, typically encompassing dimensions of less than one hundred nanometers. This multidisciplinary field spans chemistry, biology, engineering, and medicine, significantly affecting advanced materials development, medical sciences, electronics, optics, magnetism, energy storage, and electrochemistry [1]. The ability to create structures with unique properties and functionalities, unachievable through classical chemistry, positions nanotechnology at the forefront of scientific innovation. The concept of manipulating materials at atomic and molecular levels traces back to ancient times, with medieval glassmakers utilizing gold nanoparticles (NPs) to color glass [2]. NPs, typically less than one micrometer in size, exhibit distinctive physical properties due to their increased surface area-to-volume ratio and quantum effects. These properties enhance their reactivity and interaction with other materials, making them highly agglomerative. This high surface area is critical for applications such as catalysis, drug delivery, and electrode structures in energy storage devices [3].

Silica (SiO_2) is a naturally occurring compound commonly found in sand, quartz, and various living organisms. It exhibits remarkable physical and chemical stability, making it an ideal material for various applications, including catalysis, adsorption, and as a support material for nanocomposites [4]. Silica's high surface area, porosity, and biocompatibility are particularly advantageous in water treatment and biomedical applications. Traditionally, sources such as tetraethyl orthosilicate (TEOS) and sodium silicate are used in sol-gel processes to produce silica. TEOS is particularly favored for its ability to produce high-purity silica with well-defined structures. However, these conventional sources can be expensive and hazardous to handle. For instance, TEOS is a flammable liquid that requires careful handling and storage. Consequently, scientists are increasingly seeking more cost-effective and environmentally friendly alternatives for silica production [5].

One such alternative is rice husk ash (RHA), an agricultural byproduct from rice milling. RHA is rich in silica content and offers a sustainable and renewable source of SiO_2 [6]. Rice husk, an abundant agricultural waste product, is a valuable source of silica, with a content exceeding 90%. The extraction process involves controlled burning to obtain amorphous silica, which is useful in various industrial applications, including refractory materials, water purification, and concrete additives [7]. Silica

extraction from RHA provides an abundant and inexpensive source of silica and contributes to sustainable waste management practices by converting agricultural waste into valuable materials. The process typically involves pre-treatment steps such as acid leaching and thermal treatment to remove impurities and enhance silica content [8]. The resulting RHA-derived silica is characterized by its high surface area and porosity, making it suitable for synthesizing mesoporous materials [7], [9]. This method aligns with sustainable development goals by promoting the recycling of waste materials.

Magnetite (Fe_3O_4) NPs are interesting materials that exhibit unique magnetic properties due to their superparamagnetic behavior, which arises when their size is reduced to the nanometer scale. These properties include high magnetic susceptibility, rapid response to an external magnetic field, and negligible remanence when the magnetic field is removed. These characteristics make Fe_3O_4 NPs highly desirable for magnetic resonance imaging (MRI) applications, drug delivery, and environmental remediation. Moreover, their biocompatibility and ease of functionalization further enhance their utility in various biomedical and environmental technologies [10], [11]. Recent advancements in the synthesis of Fe_3O_4 NPs have focused on achieving better control over their size, shape, and magnetic properties. For instance, Hu et al. [12] reported the synthesis of Fe_3O_4 NPs via a modified co-precipitation method, resulting in particles with enhanced magnetic properties and stability. Dhao et al. [13] utilized a hydrothermal approach to synthesize Fe_3O_4 NPs with uniform size distribution and improved saturation magnetization. Aliahmad et al. [14] demonstrated the synthesis of high-quality Fe_3O_4 NPs with superior magnetic performance using thermal decomposition. These recent studies highlight the importance of precise control over synthesis conditions to optimize the performance of Fe_3O_4 NPs for various applications.

Fe_3O_4@m-SiO_2 core-shell NPs merge the magnetic properties of Fe_3O_4 with the stability and versatility of mesoporous silica (m-SiO_2). This structure features a magnetite core coated with a mesoporous silica shell, enhancing strength, providing a high surface area, allowing further functionalization, and facilitating substance loading and release. The silica shell also prevents aggregation and protects against oxidation [5]. The mesoporous silica's high surface area and porous nature are ideal for drug delivery and catalysis, enabling controlled and sustained release of substances [15], [16]. Moreover, magnetic nanoparticles (MNPs), like these superparamagnetic Fe_3O_4@m-SiO_2 particles, respond to external

3

magnetic fields. Due to their single-domain behavior and high magnetic susceptibility, they offer versatile applications, including drug delivery and MRI contrast agents.

In the current study, the synthesis and characterization of Fe_3O_4 core-shell NPs with a continuous and porous SiO_2 shell derived from RHA were explored. Using SiO_2 extracted from RHA for synthesizing $Fe_3O_4@m\text{-}SiO_2$ is a sustainable approach, turning agricultural waste into valuable nanomaterials, which is cost-effective and environmentally friendly [9], [17], [18], [19]. First, green Fe_3O_4 NPs using peppermint extract as a natural surfactant were fabricated. Then, synthesized NPs were coated with silica extracted from RHA, and superparamagnetic core-shell NPs were created. The structural integrity and surface properties were confirmed through various analytical techniques, demonstrating the NPs' potential for biomedical applications.

2- Experimental procedure

2.1 Materials

All the chemical materials used in this work were analytical grade (Merck, analytical grade). The chemicals utilized in the study include Sodium Hydroxide (NaOH) with CAS number 1310-73-2, Hydrochloric Acid (HCl) with CAS number 7647-01-0, Ammonium Hydroxide (NH_4OH) with CAS number 13366-21-6, Iron (II) Chloride ($FeCl_2$) with CAS number 7758-94-3, Iron (III) Chloride Hexahydrate ($FeCl_3 \cdot 6H_2O$) with CAS number 231-726-4, Ethanol (C_2H_6O) with CAS number 64-17-5, and Cetyltrimethylammonium Bromide (CTAB) with CAS number 57-09-0.

2.2 Extraction of Silica from Rice Husk Ash

Silica extraction from RHA was performed using an alkaline extraction method reported in our previous work [7]. Rice husks were washed with distilled water to remove impurities and then incinerated at 700 °C for 7 hours to produce ash. The ash was washed with HCl, rinsed with distilled water to a pH of 7, and dried at 90 °C for 12 hours. The dried ash was mixed with NaOH, heated until boiling with constant stirring, and then filtered. The residue was washed with warm distilled water. The resulting clear solution was cooled to room temperature. Then, HCl was added with constant stirring until the pH reached 4. The silica gel obtained was washed with distilled water and dried at 50 °C for 24 hours.

2.3 Preparation of Peppermint Leaf Extract

4

Peppermint leaf extract was prepared as an aqueous solution and was used as a natural surfactant. Initially, 10 grams of peppermint leaves were weighed and washed with distilled water. After drying, the leaves were crushed into a fine powder using a mortar and pestle [20]. Then, 250 milliliters of deionized water were added to the powder. The mixture was heated at 60-70 °C for 60 minutes. Afterward, it was filtered using Whatman filter paper No. 10, and the filtrate was used for sample preparation. The obtained extract was stored in a refrigerator.

2.4 Synthesis of Fe_3O_4@m-SiO_2 NPs

The core-shell NPs synthesis was conducted in a single step. Iron chloride powders (II and III), along with peppermint extract and a 5:1 weight percent solution of CTAB, were mixed under a nitrogen gas purge until complete dissolution of the components [21]. Then, the obtained silica powder extracted from RHA was added. Subsequently, a 2-molar solution of NH_4OH was gradually added to the initial solution until the pH reached 11. Continuous stirring was kept for 2 hours at 80 °C. During this period, the pH was supported at around 11 by adding the ammonium hydroxide solution. To study the effect of peppermint capping agent on the microstructure of Fe_3O_4 NPs, the Fe_3O_4 were fabricated using the same method, with and without peppermint extract addition during the coprecipitation synthesis process.

2.5 Materials characterization

X-ray Diffraction (XRD) was used to obtain the crystalline structure and phase composition of the samples by analyzing their diffraction patterns. Field Emission Scanning Electron Microscopy (FESEM) provided high-resolution images of the surface morphology and particle shape by employing a focused electron beam. Transmission Electron Microscopy (TEM) allowed for visualizing internal structures and particle size at the nanometer scale through electron transmission. Fourier Transform Infrared Spectroscopy (FTIR) was employed to identify functional groups and chemical bonds by measuring infrared light absorption. Dynamic Light Scattering (DLS) determined the particle size distribution in suspension by analyzing the scattered light from particle movement. Small-angle X-ray Scattering (SAXS) enabled the investigation of NP size, shape, and structural arrangement through small-angle X-ray scattering. Brunauer-Emmett-Teller (BET) Analysis was utilized to measure the surface area and porosity of the samples by analyzing nitrogen adsorption and desorption. Nitrogen

5

Adsorption-Desorption was applied to determine surface area, pore size, and porosity by measuring nitrogen gas adsorption and desorption.

3- Results and Discussion

3.1 Structural and Microstructural Analysis

XRD patterns of SiO_2, Fe_3O_4, and Fe_3O_4@m-SiO_2 NPs are shown in Fig.1a XRD spectra of extracted silica from rice husk show a broad peak centered around $2\theta = 23$ °, characteristic of amorphous silica. Therefore, the extraction and synthesis of silica in the amorphous phase were successful. For the Fe_3O_4 NPs, the diffraction peaks at 63 °, 57.5 °, 53.9 °, 43.6 °, 35.8 °, and 30.4° (2θ) correspond to the crystal planes of (220), (311), (400), (511), and (440), indicating a cubic pattern for Fe_3O_4 NPs (JCPDS NO. 19-0629). Using the Scherrer equation, the average crystallite size of approximately 11 nm was determined for the synthesized Fe_3O_4 NPs using peppermint leaf extract. For the Fe_3O_4@m-SiO_2 NPs, due to the amorphous structure of silica, the positions of the peaks are identical to those of the Fe_3O_4 NPs, but their intensities are reduced due to the silica coating and increased diameter [22]. The only difference between the XRD patterns of the coated and uncoated samples is the presence of a hump-like peak in the 20 to 30˚ region, confirming the presence of amorphous silica as a coating in the Fe_3O_4@m-SiO_2 sample.
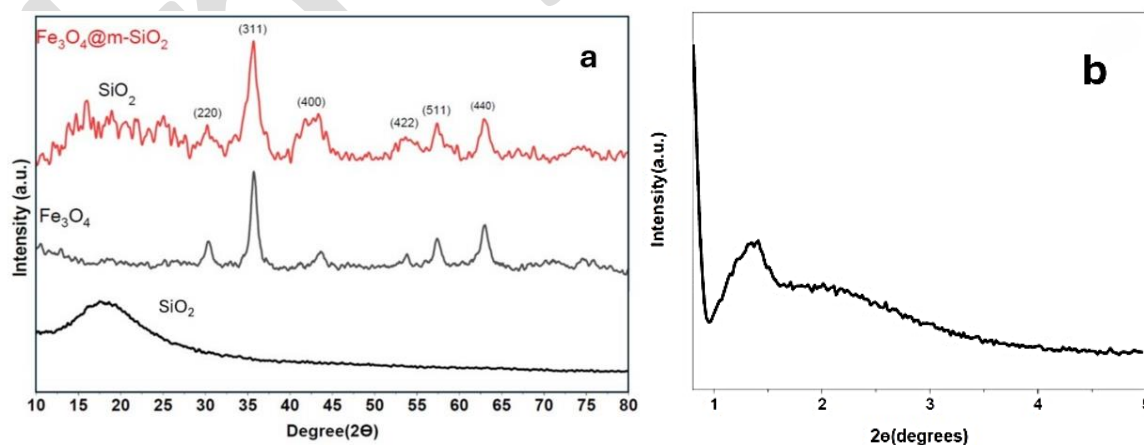

Fig. 1 (a) XRD patterns of SiO_2, Fe_3O_4, and Fe_3O_4@m-SiO_2 NPs, (b) XRD pattern at low angle of Fe_3O_4@m-SiO_2 NPs.

Low angle XRD pattern for Fe_3O_4@m-SiO_2 NPs is depicted in Fig.1b The XRD pattern shows peaks at 2θ angles of 2 °, 2.5 °, and 3 °, with a well-defined peak at 1.5 ° and a broad peak in between these angles. These results confirm the mesoporous nature of the silica and indicate a relatively regular pore structure. The observed peaks are consistent with findings reported in other studies [23].

FTIR Spectroscopy is used to investigate functional groups formed in materials. Fig. 2 shows the FTIR spectrum of SiO_2, Fe_3O_4, and Fe_3O_4@m-SiO_2 NPs. A broad peak between 3000-3600 cm⁻¹ is observed for silica extracted from RHA, corresponding to the vibrational bonding of OH groups absorbed by silica molecules [24]. This indicates a significant presence of absorbed water in the synthesized silica. Absorption peaks at 800-460 cm⁻¹ correspond to O-Si bonds, and the peak at 1080 cm⁻¹ correspond to Si-O-Si bonds [25]. For magnetite NPs, the absorption bands at 3430 cm⁻¹ and 1620 cm⁻¹ are related to hydroxyl compounds, while those at 570 cm⁻¹ and 1250 cm⁻¹ correspond to Fe-O stretching [26]. For Fe_3O_4@m-SiO_2 NPs peaks at 460 cm⁻¹ and 800 cm⁻¹ are associated with O-Si stretching, while the peak at 1080 cm⁻¹ is related to Si-O-Si stretching, confirming the presence of a silica coating on the Fe_3O_4 NPs [27]. Additionally, the peak at 950 cm⁻¹ corresponds to OH-Si bonds on the NPs surfaces. The broad peak in the range of 3600-3000 cm⁻¹ in the spectrum indicates hydrogen bond vibrations, reflecting the presence of hydroxyl groups and O-H on the surface of the synthesized NPs [28], [29]. The peak at 570 cm⁻¹ is attributed to Fe-O-Si bonds, resulting from the close proximity and linking of silica and iron [26]. Carbonaceous bonds observed in the spectrum are due to the presence of organic material from the mint extract used during the synthesis of pure magnetite NPs and core-shell NPs, with some residues remaining in the system despite washing. This vibration may also be due to the presence of water molecules in the sample. The peak at 1645 cm⁻¹ in the spectrum of Fe_3O_4@m-SiO_2 NPs indicates the presence of H-O bonds, demonstrating successful functionalization of the Fe_3O_4@m-SiO_2 NPs [30], [31].

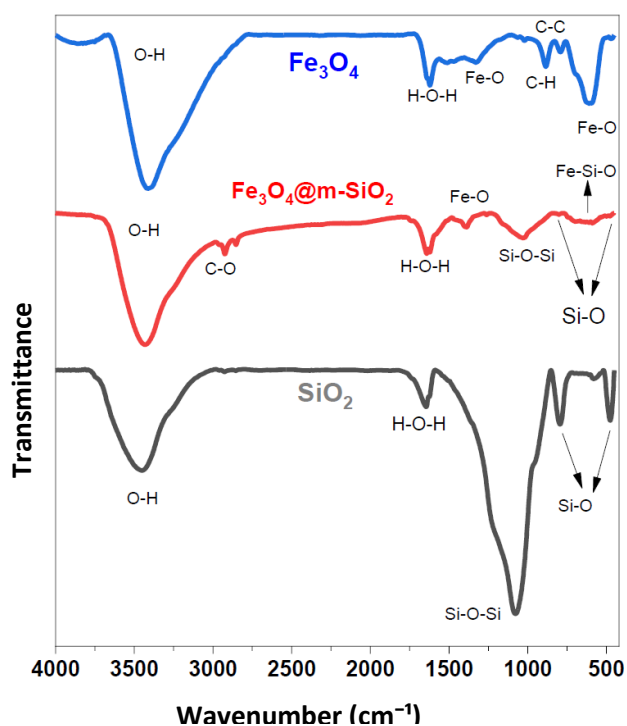Fig. 2. FTIR spectra of SiO_2, Fe_3O_4, Fe_3O_4@m-SiO_2 NPs.

As previously mentioned, to study the effect of peppermint capping agent on the microstructure of Fe_3O_4 NPs, the Fe_3O_4 were fabricated using the same method, with and without peppermint extract addition during the coprecipitation synthesis process. The FESEM image of the synthesized Fe_3O_4 NPs with and without capping agent are shown in Fig. 3a and 4b, respectively. The magnetic particle shapes in both conditions are nearly spherical, but in the first condition, the particle size is finer with a more uniform size distribution (21.3 ± 2.6 nm), showing the effectiveness of peppermint extract as a spatial hindrance creating additive. The SEM micrographs of Fe_3O_4@m-SiO_2 NPs are shown in Fig. 3c and 4d. According to the obtained images, MNPs synthesized with peppermint extract and coated with silica show a morphology tending toward spherical. Particle size distribution and average particle size, considering 200 particles using Image J software, have been figured out. The average size of Fe_3O_4 NPs is 19.6 nm, and for Fe_3O_4@m-SiO_2 NPs, it is 45.8 nm.

The elemental maps of Fe_3O_4@m-SiO_2 NPs generated by EDS analysis are shown in Fig. 4. The presence of all elements and their homogeneous distribution in the synthesized sample can be

8

confirmed. As shown in the images, the elements Fe, Si, and O are well-distributed in the synthesized

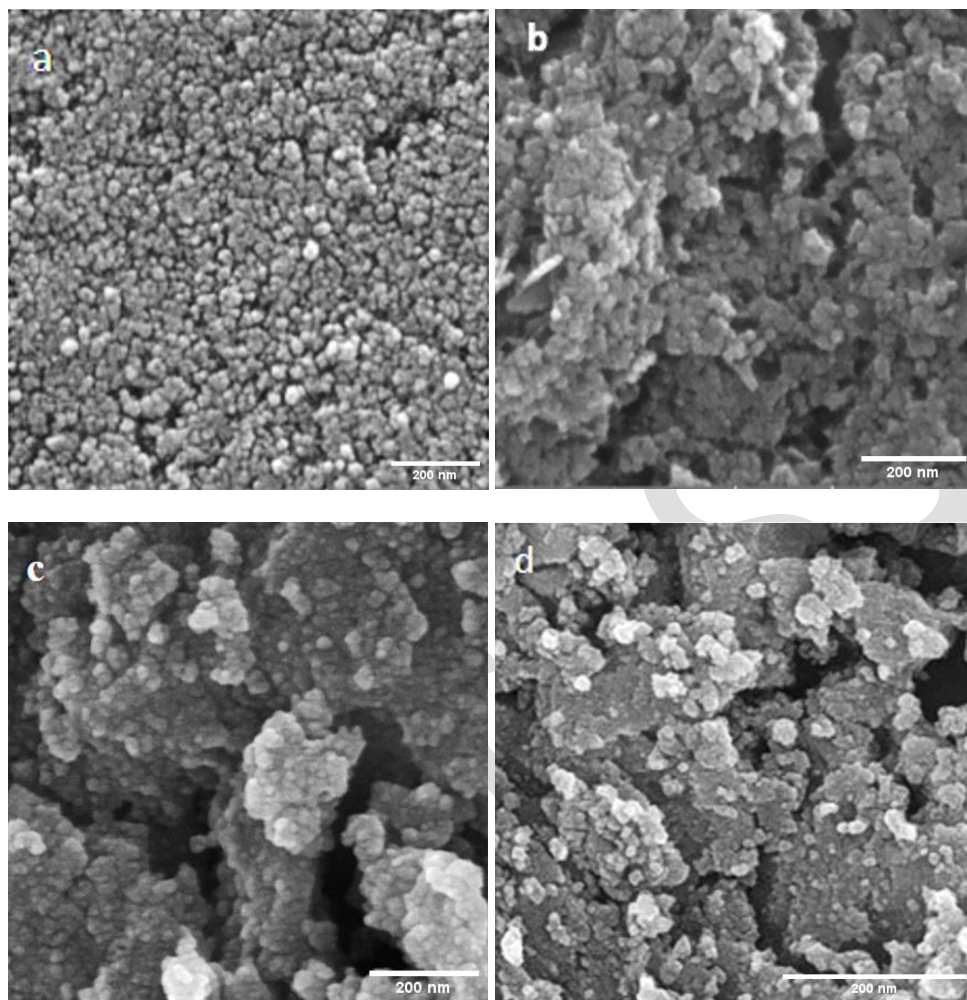sample, indicating a homogeneous distribution of silica in the magnetite.

Fig. 3. FESEM image of (a) Fe_3O_4 NPs synthesized with peppermint extract, (b) Fe_3O_4 NPs without
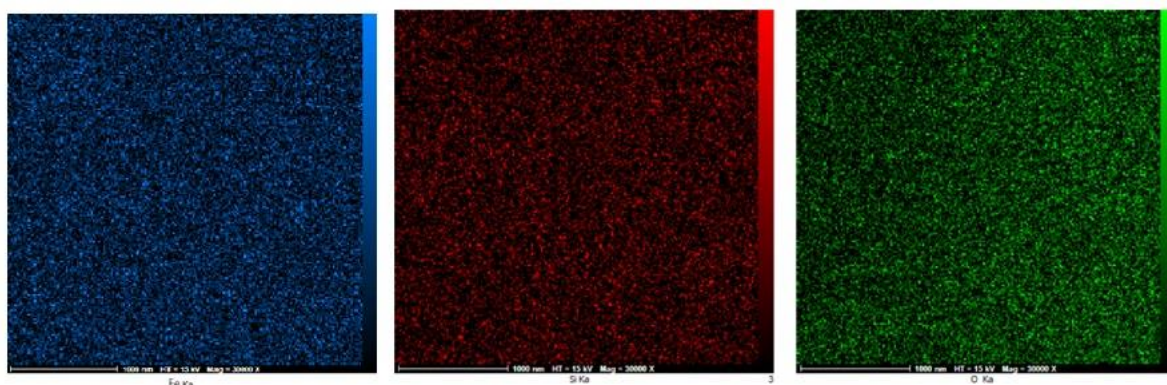
peppermint extract, (c) and (d) Fe_3O_4@m-SiO_2 NPs.

Fig. 4. Elemental Mapping Images of Fe_3O_4@m-SiO_2 NPs.

9

TEM micrographs of the Fe_3O_4@m-SiO_2 sample are illustrated in Fig. 5. The corresponding images verify the presence of silica coating on iron oxide NPs. However, it can be observed that the synthesized core-shell NPs are multi-core. The presence of hollow-like structures on the outer surface of the particle is due to the porous structure in the outer shell.
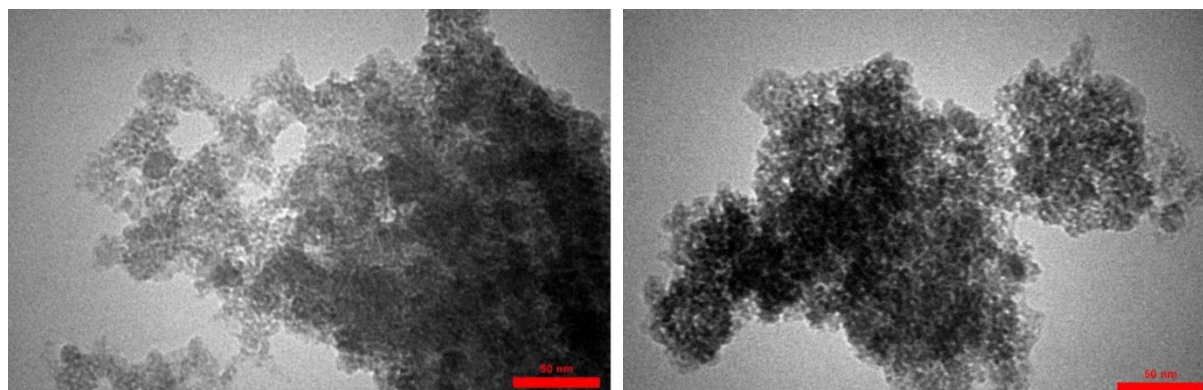

Fig. 5. TEM images of Fe_3O_4@m-SiO_2 NPs.

The results obtained from the DLS test are presented in Fig. 6, showing the hydrodynamic size distribution and frequency of particles forming the sample. It can be seen that the synthesized Fe_3O_4@m-SiO_2 NPs show a relatively narrow size distribution, with an average particle size of 72.6 nanometers. In this sample, the PDI is 0.6, indicating some agglomerated NPs.
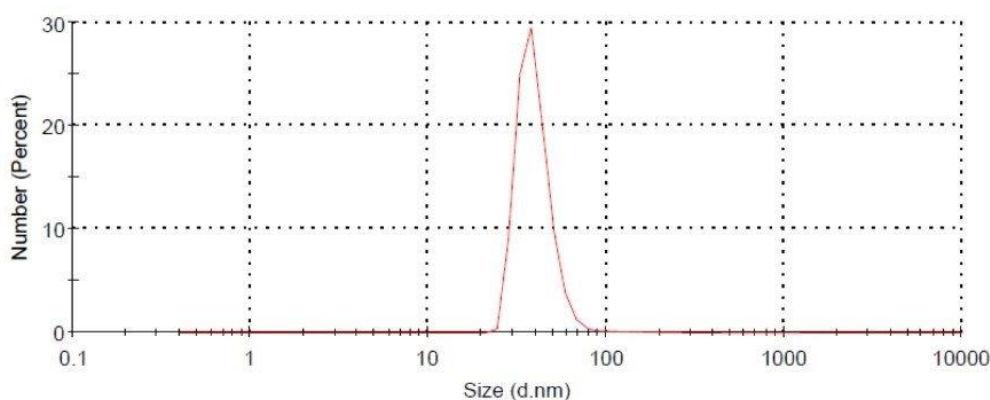

Fig. 6. Hydrodynamic particle size distribution.

Using data related to the volume of gas absorbed on the surface of the porous material at different relative pressures, valuable information such as specific surface area, volume, size, and pore size distribution can be obtained. Additionally, by examining the shape of the adsorption-desorption curve,

10

one can estimate the shape of the porous material [32]. Based on the nitrogen adsorption-desorption isotherms and BET plots presented in Fig. 7, it has been determined that the specific surface area of the $Fe_3O_4@m\text{-}SiO_2$ NPs is 323.92 m^2/gr and the pore volume is 0.46 cm^3/gr with 0.06 cm^3/gr pore size attributed to micropores. These values closely match the reported values. Additionally, considering the pore size distribution diagram shown in Fig. 7, the average pore size in the synthesized mesoporous material is 5.07 nm. According to the nitrogen adsorption-desorption pattern, this mesoporous material conforms to the IUPAC definition and falls under Group IV, similar to magnetic silica mesoporous MCM-41, demonstrating the successful synthesis of this mesoporous material. Moreover, the loop shape obtained in the adsorption-desorption curve of the synthesized sample indicates that the shape of the pores is a combination of cylindrical and slit-like structures [32].
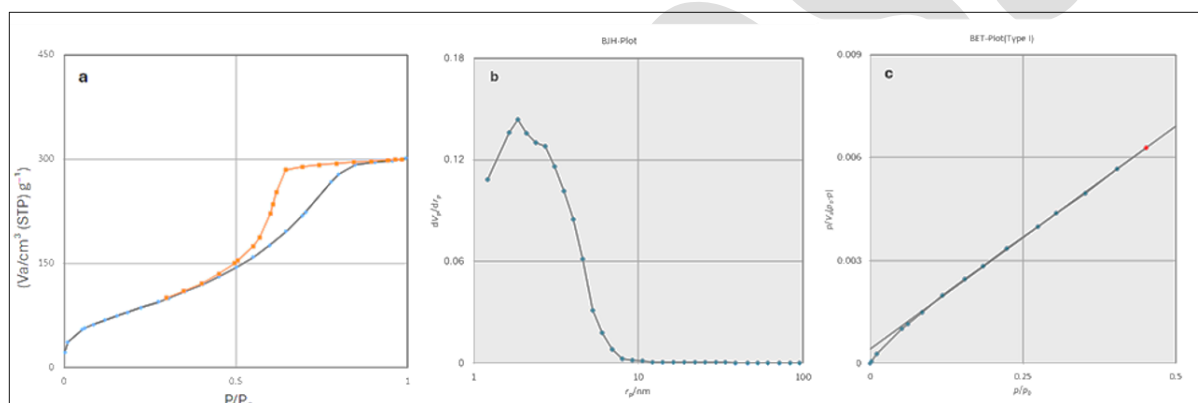

Fig. 7. (a) Nitrogen Adsorption-Desorption Isotherm of $Fe_3O_4@m\text{-}SiO_2$ NPs, (b) The pore size distribution plot of the Fe_3O_4 m-SiO_2 NPs, and (c) The BET plot of the $Fe_3O_4@m\text{-}SiO_2$ NPs.

3.2 Magnetic Characteristics

To investigate the magnetization curves of the Fe_3O_4 samples, a VSM method was used, as shown in Fig. 8. The results indicate that the samples are superparamagnetic, with a saturation magnetization of 27.5 emu/g for the $Fe_3O_4@m\text{-}SiO_2$ sample. For the Fe_3O_4 sample without the SiO_2 coating, the saturation magnetization is 57.9 emu/g, which is higher than the coated sample but lower than the bulk Fe_3O_4 (approximately 60-80 emu/g) [33]. This reduction in specific magnetization for the coated sample is attributed to various factors, including particle size and the mass of the non-magnetic porous material. The decrease in specific magnetization in the coated sample is due to the presence of the mineral

11

coating. SiO_2 molecules adsorbed on the surface of the Fe_3O_4 NPs attract oxygen atoms, which are sources of magnetic moments on the surface. However, these oxygen atoms cannot contribute to the overall magnetization as they did before, leading to a reduction in the magnetization of the coated NPs [27,34,35]. Studies have shown that an increase in the surface-to-volume ratio and significant surface effects in NPs, compared to bulk structures, results in a decrease in the magnetization of the NPs. This reduction can be attributed to the presence of magnetically dead layers on the particle surfaces and an increase in the disparity between surface anisotropy energy and bulk magnetostatic energy due to canted spins and oxide layers [36].
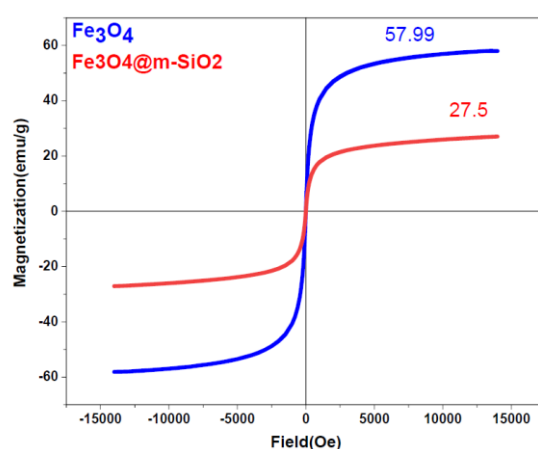

Fig. 8. VSM comparative diagram of Fe_3O_4 and $Fe_3O_4@m\text{-}SiO_2$ NPs.

4- Conclusions

This study successfully employed a green synthesis approach using mint extract as a natural surfactant and RHA as a silica source to create superparamagnetic magnetite core-shell NPs with a mesoporous silica shell. The synthesis process proved cost-effective and environmentally friendly, producing NPs with potential biomedical applications. XRD and FT-IR analyses confirmed the formation of the desired crystalline structures and the successful incorporation of silica. SEM, TEM, and DLS tests further confirmed the presence of mesoporous silica coating, with the average sizes of core-shell NPs measured at 72.6 nm. The use of peppermint as a capping agent significantly enhances the synthesis of Fe_3O_4 NPs, ensuring their homogeneity and monodispersity. BET analysis showed a high surface area of 323.92 m²/g, highlighting the effective synthesis of a porous silica coating. The VSM results show that

12

Fe$_3$O$_4$@m-SiO$_2$ samples are superparamagnetic with a specific magnetization of 27.5 emu/g, reduced from 57.9 emu/g in uncoated Fe$_3$O$_4$ due to the SiO$_2$ coating and surface effects. This research underscores the feasibility and advantages of using natural materials for sustainable nanoparticle synthesis. According to the results of this research, the synthesized Fe$_3$O$_4$@m-SiO$_2$ nanocomposites, utilizing silica extracted from RHA, exhibit superparamagnetic properties and successful mesoporous coating on magnetites. These characteristics make them highly suitable for potential applications in targeted drug delivery, magnetic resonance imaging (MRI), environmental remediation, and water treatment due to their high stability, biocompatibility, responsiveness to external magnetic fields, and high surface area.

Acknowledgement

References

1. Horcajada, P., Chalati, T., Serre, C., Gillet, B., Sebrie, C., Baati, T., Eubank, J. F., Heurtaux, D., Clayette, P., Kreuz, C., Chang, J.-S., Hwang, Y. K., Marsaud, V., Bories, P.-N., Cynober, L., Gil, S., Férey, G., Couvreur P. and Gref R., "Porous metal-organic-framework nanoscale carriers as a potential platform for drug delivery and imaging," *Nat. Mater.*, 2010, 9(2), 172–178.

2. Chakraborty, A., Roy, T., and Mondal, S., "Development of DNA Nanotechnology and Uses in Molecular Medicine and Biology," *Insights Biomed.*, 2016, 1(2), 1–10.

3. Sahoo, S. K., and Labhasetwar, V., "Nanotech approaches to drug delivery and imaging," *Drug Discov. Today*, 2003, 8(24), 1112–1120.

4. Janasree, P. and Kumar, M. K., "Synthesis and Characterization of Nanosilica from Rice Husk Ash Prepared by Precipitation Method for Chemically Synthesized Nanocement," *J. Emerg. Technol. Innov. Res.*, 2018, 5(8), 314–318.

5. Azadpour, B., Aharipour, N., Paryab, A., Omid, H., Abdollahi, S., Madaah Hosseini, S., Malek Khachatourian, A., Toprak, M. S., and Seifalian, A. M., "Magnetically-assisted viral transduction (magnetofection) medical applications: An update," *Biomater. Adv.*, 2023, 53, 213657.

13

6. Alshatwi, A. A., Athinarayanan, J., and Periasamy, V. S., "Biocompatibility assessment of rice husk-derived biogenic silica nanoparticles for biomedical applications," *Mater. Sci. Eng. C*, 2015, 47, 8–16.

7. Aharipour, N., Nemati, A., & Khachatourian, A. M., "Green Synthesis of Silica Extracted from Rice Husk Ash," *Adv. Ceram. Prog.*, 2022, 8(4), 15–20.

8. Kalapathy, U., Proctor, A., & Shultz, J., "A simple method for production of pure silica from rice hull ash," *Bioresour. Technol.*, 2000, 73(3), 257–262.

9. Chakraverty, A., and Kaleemullah, S., "Conversion of rice husk into amorphous silica and combustible gas," *Energy Convers. Manag.*, 1991, 32(6), 565–570.

10. Laurent, S., Forge, D., Port, M., Roch, A., Robic, C., Vander Elst, L., and Muller, R. N., "Magnetic iron oxide nanoparticles: Synthesis, stabilization, vectorization, physicochemical characterizations, and biological applications," *Chem. Rev.*, 2008, 108(6), 2064–2110.

11. Wu, W., He, Q., & Jiang, C., "Magnetic iron oxide nanoparticles: Synthesis and surface functionalization strategies," *Nanoscale Res. Lett.*, 2008, 3(11), 397–415.

12. Hui, C., Shen, C., Tian, J., Bao, L., Ding, H., Li, C., Tian, Y., Shia, X., and Gao H.-J., "Core-shell Fe3O4@SiO2 nanoparticles synthesized with well-dispersed hydrophilic Fe3O4 seeds," *Nanoscale*, 2011, 3, 701–705.

13. Daou, T. J., Pourroy, G., Bégin-Colin, S., Grenèche, J. M., Ulhaq-Bouillet, C., Legaré, P., Bernhardt, P., Leuvrey, C., and Rogez, G., "Hydrothermal synthesis of monodisperse magnetite nanoparticles," *Chem. Mater.*, 2006, 18(18), 4399–4404.

14. Aliahmad, M., and Nasiri Moghaddam, N., "Synthesis of maghemite (γ-Fe2O3) nanoparticles by thermal-decomposition of magnetite (Fe3O4) nanoparticles," *Mater. Sci. Pol.*, 2013, 31(2), 264–268.

15. Chomoucka, J., Drbohlavova, J., Huska, D., Adam, V., Kizek, R., and Hubalek, J., "Magnetic nanoparticles and targeted drug delivering," *Pharmacol. Res.*, 2010, 62(2), 144–149.

16. Harris, L. A., Goff, J. D., Carmichael, A. Y., Riffle, J. S., Harburn, J. J., Pierre, T. G. St., and Saunders, M., "Magnetite nanoparticle dispersions stabilized with triblock copolymers," *Chem. Mater.*, 2003, 15(6), 1367–1377.

17. Nzereogu, P.U., Omah, A.D., Ezema, F.I., Iwuoha, E.I., and Nwanya, A.C., "Silica extraction from rice husk: Comprehensive review and applications," *Hybrid Advances*, 2023, 4, 100111.

18. Real, C., Alcala, M. D., and Criado, J. M., "Preparation of Silica from Rice Husks," *J. Am. Ceram. Soc.*, 1996, 79(8), 2012–2016.

19. Adira Jaafar, J., Hidayatul Nazirah Kamarudin, N., Dina Setiabudi, H., Najiha Timmiati, S., and Lee Peng, T., "Mesoporous Silica Nanoparticles and Waste Derived-Siliceous Materials for Doxorubicin Adsorption and Release," *Mater. Today Proc.*, 2019, 19, 1420–1425.

20. Sroka, Z., Fecka, I., and Cisowski, W., "Antiradical and Anti-H2O2 Properties of Polyphenolic Compounds from an Aqueous Peppermint Extract," *Zeitschrift fur Naturforsch. - Sect. C J. Biosci.*, 2005, 60(11–12), 826–832.

21. Thanh, L. H. V. T., Lan, N. P., Quyen, T. T. B., Nam, H. Q., and Tho, L. P. B., "Synthesis and Characterization of Fe3O4@SiO2 Sub-Nano core/Shell With SiO2 Derived from Rice Husk Ash," *The University of Danang - Journal of Science and Technology*, 2020, 18(16), 52-56.

22. Chhabra, V., Ayyub, P., Chattopadhyay, S., and Maitra, A. N., "Preparation of acicular γ-Fe₂O₃ particles from a microemulsion-mediated reaction," *Mater. Lett.*, 1996, 26(1–2), 21–26.

23. Dhal, J. P., Dash, T., and Hota, G., "Iron oxide impregnated mesoporous MCM-41: synthesis, characterization and adsorption studies," *J. Porous Mater.*, 2020, 27(1), 205–216.

24. Srivastava, V. C., Mall, I. D., and Mishra, I. M., "Characterization of mesoporous rice husk ash (RHA) and adsorption kinetics of metal ions from aqueous solution onto RHA," *J. Hazard. Mater.*, 2006, 134(1–3), 257–267.

25. Asadi, F., Shariatmadari, H., and Mirghaffari, N., "Modification of rice hull and sawdust sorptive characteristics for remove heavy metals from synthetic solutions and wastewater," *J. Hazard. Mater.*, 2008, 154(1–3), 451–458.

26. Castillo, J., Vargas, V., Macero, D., Le Beulze, A., Ruiz, W. and Bouyssiere, B., "One-step synthesis of SiO₂ α−Fe₂O₃ / Fe₃O₄ composite nanoparticles with magnetic properties from rice husks," *Phys. B Condens. Matter*, 2021, 605, 412799.

27. Davaran, S., Akbarzadeh, A., Nejati-Koshki, K., Alimohammadi, S., Farajpour Ghamari, M., Mahmoudi Soghrati, M., Rezaei, A., and Khandaghi, A. A., "In Vitro Studies of NIPAAM-MAA-

15

VP Copolymer-Coated Magnetic Nanoparticles for Controlled Anticancer Drug Release," *J. Encapsulation Adsorpt. Sci.*, 3(4), 2013, 108–115.

28. Kayal, S., and Ramanujan, R. V., "Anti-cancer drug loaded iron-gold core-shell nanoparticles (Fe@Au) for magnetic drug targeting," *J. Nanosci. Nanotechnol.*, 2010, 10(9), 5527–5539.

29. Sahin, F., Turan, E. Tumturk, H., and Demirel, G., "Core-shell magnetic nanoparticles: A comparative study based on silica and polydopamine coating for magnetic bio-separation platforms," *Analyst*, 2012, 137(23), 5654–5658.

30. Kayal, S., and Ramanujan, R. V., "Doxorubicin loaded PVA coated iron oxide nanoparticles for targeted drug delivery," *Mater. Sci. Eng. C*, 2010, 30(3), 484–490.

31. Mahmoudi, M., Simchi, A., Imani, M., and Hafeli, U. O., "Superparamagnetic iron oxide nanoparticles with rigid cross-linked polyethylene glycol fumarate coating for application in imaging and drug delivery," *J. Phys. Chem. C*, 2009, 113(19), 8124–8131.

32. Thommes, M., Kaneko, K., Neimark, A. V., Olivier, J. P., Rodriguez-Reinoso, F., Rouquerol, J., and Sing, K. S.W., "Physisorption of gases, with special reference to the evaluation of surface area and pore size distribution (IUPAC Technical Report)," *Pure Appl. Chem.*, 2015, 87(9–10), 1051–1069.

33. Peng, H., Hu, C., Hu, J., Tian, X., and Wu, T., "Fe3O4@mZnO nanoparticles as magnetic and microwave responsive drug carriers," *Microporous Mesoporous Mater.*, 2016, 226, 140–145.

34. Li, F., Li, X., and Li, B., "Preparation of magnetic polylactic acid microspheres and investigation of its releasing property for loading curcumin," *J. Magn. Magn. Mater.*, 2011. 323(22), 2770–2775.

35. K. B. Narayanan and N. Sakthivel, "Biological synthesis of metal nanoparticles by microbes," *Adv. Colloid Interface Sci.*, 2010,156(1–2), 1–13.

36. Sunitha, A., Rimal1, I. R. S., Sweetly, G., Sornalekshmi, S., Arsula, R., and Praseetha, P. K., "Evaluation of antimicrobial activity of biosynthesized iron and silver nanoparticles using the fungi fusarium oxysporum and actinomycetes sp. on human pathogens," *Nano Biomed. Eng.*, 2013, 5(1), 39–45.